

Review

Cu_xO Nanostructure-Based Gas Sensors for H₂S Detection: An Overview

Sachin Navale^{1,2,3,†}, Mehrdad Shahbaz^{4,†}, Sanjit Manohar Majhi^{1,3}, Ali Mirzaei^{5,*} , Hyoun Woo Kim^{1,2,*} and Sang Sub Kim^{3,*} 

¹ Division of Materials Science and Engineering, Hanyang University, Seoul 04763, Korea; stnavale2@yahoo.com (S.N.); jeetmjh@gmail.com (S.M.M.)

² The Research Institute of Industrial Science, Hanyang University, Seoul 04763, Korea

³ Department of Materials Science and Engineering, Inha University, Incheon 22212, Korea

⁴ Department of Materials Science and Engineering, Faculty of Engineering, Urmia University, Urmia 5756-151818, Iran; m.shahbaz@urmia.ac.ir

⁵ Department of Materials Science and Engineering, Shiraz University of Technology, Shiraz 715557-13876, Iran

* Correspondence: mirzaei@sutech.ac.ir (A.M.); hyounwoo@hanyang.ac.kr (H.W.K.); sangsub@inha.ac.kr (S.S.K.)

† These authors contributed equally to this work.

Abstract: H₂S gas is a toxic and hazardous byproduct of the oil and gas industries. It paralyzes the olfactory nerves, with concentrations above 100 ppm, resulting in loss of smell; prolonged inhalation may even cause death. One of the most important semiconducting metal oxides for the detection of H₂S is Cu_xO (x = 1, 2), which is converted to Cu_xS upon exposure to H₂S, leading to a remarkable modulation in the resistance and appearance of an electrical sensing signal. In this review, various morphologies of Cu_xO in the pristine form, composites of Cu_xO with other materials, and decoration/doping of noble metals on Cu_xO nanostructures for the reliable detection of H₂S gas are thoroughly discussed. With an emphasis to the detection mechanism of Cu_xO-based gas sensors, this review presents findings that are of considerable value as a reference.

Keywords: gas sensor; H₂S gas; Cu_xO; Cu_xS; sensing mechanism



Citation: Navale, S.; Shahbaz, M.; Majhi, S.M.; Mirzaei, A.; Kim, H.W.; Kim, S.S. Cu_xO Nanostructure-Based Gas Sensors for H₂S Detection: An Overview. *Chemosensors* **2021**, *9*, 127. <https://doi.org/10.3390/chemosensors9060127>

Academic Editors:

Bilge Saruhan-Brings, Roussin

Lontio Fomekong and

Svitlana Nahirniak

Received: 7 April 2021

Accepted: 30 May 2021

Published: 2 June 2021

Publisher's Note: MDPI stays neutral with regard to jurisdictional claims in published maps and institutional affiliations.



Copyright: © 2021 by the authors. Licensee MDPI, Basel, Switzerland. This article is an open access article distributed under the terms and conditions of the Creative Commons Attribution (CC BY) license (<https://creativecommons.org/licenses/by/4.0/>).

1. Overview of H₂S Gas Properties

H₂S, which has a disagreeable odor, is a colorless, highly toxic, corrosive, flammable, and explosive gas [1,2]. It has various sources, including volcanic eruptions, anaerobic decay of organic materials, Kraft paper mills, processing of gasoline, natural gas, coal, and sewage, as well as petroleum refining [3–6]. Other sources of H₂S include decomposition of fish in the fishing industry and waste biodegradation in shrimp farms [7]. H₂S is readily oxidized by atmospheric oxygen when irradiated with sunlight and can form SO₂ and H₂SO₄ in the atmosphere, leading to acid rains [8]. Moreover, because H₂S is heavier than air, it remains in the atmosphere for up to 18 h; thus, it can easily accumulate in areas such as mine tunnels, sewers, and manure tanks [9,10]. As stated by the *United States Occupational Safety and Health Administration* (US-OSHA, Washington, DC, USA), the concentration limit for exposure to H₂S within 8 h is approximately 20 ppm [11]. Exposure to low levels of H₂S may result in eye and throat injuries, dizziness, memory impairment, and loss of reasoning and balance [12–15]. Continuous exposure to H₂S at 2 ppm causes nausea/headaches, while 20 ppm results in fatigue and headache, and concentrations of 50–100 ppm result in loss of appetite, respiratory tract irritation, digestion issues, and loss of breathing with high possibility of death [13,16]. Moreover, an individual's olfaction may quickly fail to function properly when exposed to H₂S levels of more than 100 ppm for a short period of time [17]. Prolonged exposure to 100 ppb of H₂S also affects respiration in human cells and causes a deficiency of oxygen in systemic tissues, endangering human health [18,19]. H₂S exposure at concentrations of 1000 ppm and above would result in

immediate death. For example, 21 fatalities were reported in the Gulf of Mexico in 2007 as a result of H₂S leaks and chain accidents on the Kab-121 platform [20]. In addition, H₂S is a known biomarker for various diseases such as Down syndrome, Alzheimer's disease, ischemia, asthma, and halitosis [21]. For example, the H₂S concentration (~100–500 ppb) in the breath of patients with halitosis is greater than that in healthy individuals. This is primarily due to local oral diseases and certain systemic diseases, such as digestive issues [22]. Accordingly, detection of H₂S gas is important from the perspectives of safety, industry, and medicine.

2. Motivation for the Use of Cu_xO as a H₂S Gas Sensor

To date, several types of gas sensors, including chemoresistive gas sensors made of semiconducting metal oxides, electrochemical sensors, optical sensors, and piezoelectric sensors, have been utilized for H₂S gas detection [23–25]. Among them, semiconducting metal oxide gas sensors are widely popular owing to their advantages such as simple operation, small size, low cost, high sensitivity, high stability, fast response, and long life [26,27]. Overall, the sensing mechanism in this type of gas sensor is the change in resistance caused by exposure to target gases [28,29]. The gas response depends mainly on the contact between the target gases and the surface of the sensing element, as well as the adsorption sites on the sensor surface [30]. Among the different metal oxides used for H₂S-sensing, Cu_xO (x = 1, 2) is an exception. CuO is a low-cost semiconducting metal oxide (energy gap = 1.2 eV) and has a monoclinic crystal structure [31]. It can directly react with H₂S to form a Cu_xS layer with high conductivity. Primarily, CuS forms clusters on the surface of CuO, which grows progressively and links to create a persistent CuS phase with metallic-like conductivity. This process generates a conductive percolation pathway, which consequently decreases the resistance abruptly [32]. The electrons flow from CuO to CuS owing to the difference in their work functions and formation of a potential barrier. When the grain boundaries transform into CuS, the width of the potential barrier is minimized, and the conductivity changes from semiconducting to metallic, resulting in an advanced H₂S response [33]. Thus, Cu_xO is highly popular for H₂S gas-sensing studies [12,26,34]. Furthermore, it can be used as an adsorbent for the purification of gas streams, especially by H₂S removal [35]. In addition, the selectivity of Cu_xO can be related to the lower bond energy of H₂S relative to other gases. As shown in Table 1, the H-SH bonding energy in H₂S is 381 kJ/mol, which is lower than that of most interfering gases, leading to better interaction and dissociation of the surface of the sensing material.

Table 1. Various gas molecules and their properties [36].

Gas	Ammonia (NH ₃)	Hydrogen (H ₂)	Methane (CH ₄)	Carbon Monoxide (CO)	H ₂ S
Bond	H-NH ₂	H-H	H-CH ₃	C-O	H-SH
Bond Energy (kJ/mol)	435	436	431	1076	381
Molecular Size (nm)	0.26	0.289	0.38	0.37	0.34

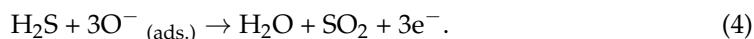
3. Gas Sensors Based on Pristine Cu_xO Nanostructures

Hu et al. [37] conducted a study on the magnetron sputtering of p-type CuO nanoneedle arrays followed by wet chemical etching and annealing. Their CuO sensor demonstrated a response of 76.5% ($\Delta R/R_a$) × 100 to 15 ppm H₂S gas at 150 °C. The oxygen molecules from air are adsorbed onto the sensor surface to form a hole accumulation layer (HAL); thereafter, the sensor resistance decreases relative to vacuum because of the adsorption of electrons as follows [37]:





When the sensor is in an H_2S atmosphere, the chemical reaction between the adsorbed H_2S molecules on the sensor surface and the chemisorbed oxygen species occurs as follows:



The released electrons are combined with holes, and the thickness of the HAL decreases. Thus, the resistance increases, which leads to the appearance of a sensing signal. However, the authors did not report the formation of CuS , and the selectivity of the gas sensor was not explained. In another study, Huang et al. synthesized sea anemone-like CuO nanoarrays in situ via a seed-induced hydrothermal method at different time durations (1–6 h) [38]. For growth times exceeding 2 h, they observed that the CuO nanostructures grew among the electrodes, and CuO nanostructures and sea anemone array morphologies were formed. The surface areas of CuO nanoarrays prepared for 2, 3, 4, 5, and 6 h were 5.85, 7.35, 7.03, 6.67, and 5.70 $\text{m}^2 \cdot \text{g}^{-1}$, respectively. The surface area decreased with increasing growth time (>2 h). The results of H_2S gas-sensing showed that the CuO prepared for 2 h had the lowest response among the other sensors because of the fragile continuity of the tiny CuO nanoarrays, which did not offer the active electrical conduction pathways necessary for the H_2S -sensing reactions. The sensor with the largest surface area (prepared for 3 h) showed not only the highest response to H_2S gas (24.08 to 5 ppb H_2S gas at 25 °C), but also good selectivity, as shown in Figure 1a.

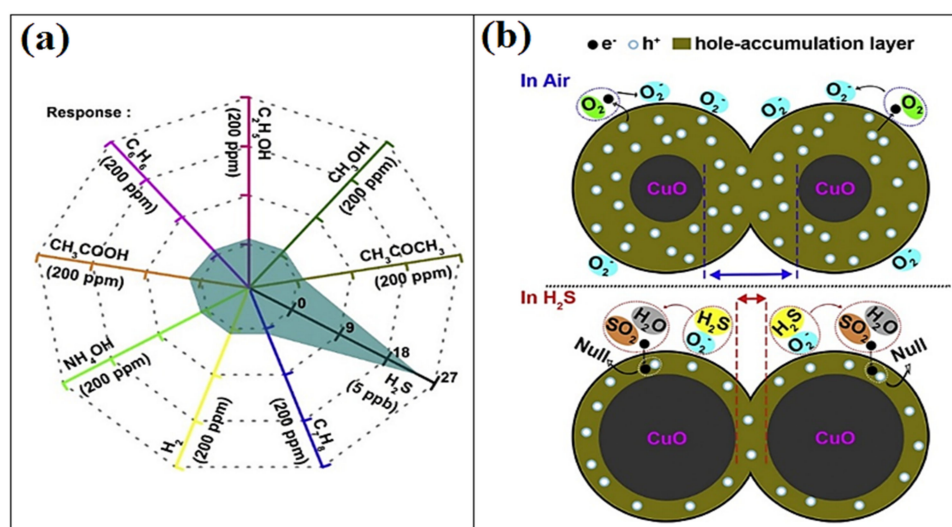


Figure 1. (a) Selectivity pattern of the p-CuO gas sensor prepared for 3 h to various gases at 25 °C in 34% RH; (b) schematic of the width variation of HAL when exposed in air and H_2S . Reprinted from [38] with permission from Elsevier.

As shown in Figure 1b the HAL was formed in air, and the oxygen adsorption made it wider at the junctions, which enabled hole transmission and subsequently decreased the resistance. In the H_2S gas atmosphere, the HAL was narrowed, which hampered the transmission of holes while the sensor resistance increased. In addition, the cross-linked assembly enabled the adsorption, dispersion, and channeling of H_2S molecules in detecting reactions and efficiently evaded the lateral stacking and accumulation of CuO nanostructures with no specific surface area loss because of the slight contact and appropriate clearance. This eventually led to a high sensitivity of the gas sensor toward H_2S gas.

As humidity is always present in real environments, the development of gas sensors that can operate under humid conditions is important. Accordingly, Miao et al. [39] described the humidity-independent H_2S -sensing performance of hydrothermally processed

monolayered CuO nanosheet films under dry and wet conditions. Figure 2a,b compares the sensing mechanism of the CuO gas sensor to H₂S in dry and humid environments. In particular, in the humid state, previously adsorbed oxygen anions are substituted partly via terminal hydroxyl groups, which results in low reactions between H₂S molecules and chemisorbed oxygen atoms. The extent of this limit was determined on the basis of the humidity level in the gas chamber. Accordingly, the sensor signal to H₂S decreased steadily as the humidity level increased. However, in H₂S-sensing, the inclusion of S in the CuO framework was assisted by the terminal hydroxyl group at the surface. In addition, the higher humidity level resulted in an abundance of terminal hydroxyl groups, and, as a result, greater conversion from CuO to Cu₂S and S occurred. This was due to variable oxidation states of Cu and was demonstrated by XPS and SEM studies. Thus, the sensor response was maintained at the same level as the humidity increased. The decreased recovery time observed under humid conditions was elucidated through the low thermal stability of Cu₂S. The characteristic Gibbs free energies for the development for CuO, Cu₂O, and Cu₂S were −129.7 kJ/mol, −146.0 kJ/mol, and −86.2 kJ/mol, respectively. In this way, changing from a less thermodynamically steady phase (i.e., Cu₂S) into CuO would be a much more straightforward process than from a steady phase (Cu₂O); accordingly, a quicker recovery time was observed under humid conditions [39].

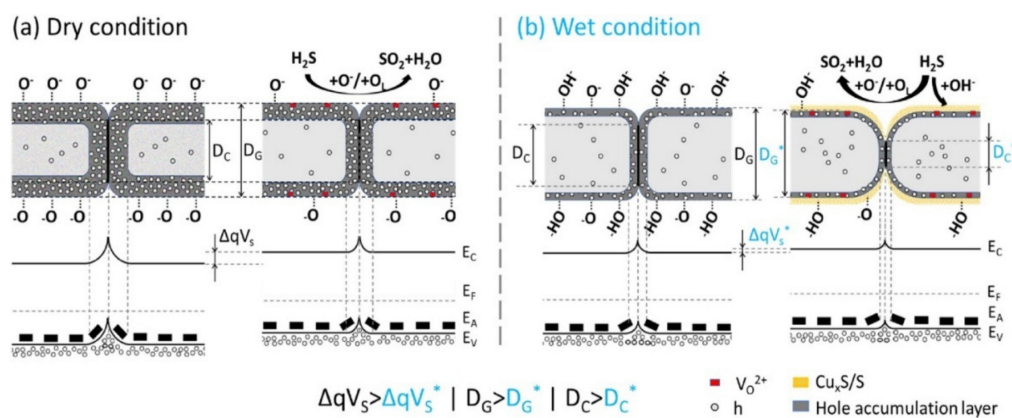


Figure 2. Schematic of H₂S detecting mechanism of p-CuO nanosheet gas sensor in (a) dry and (b) humid environments. Reprinted from [39] with permission from Elsevier.

Dhakshinamoorthy et al. [40] described the H₂S gas-sensing features of CuO nanocuboids. The fabricated CuO nanocuboid sensor had a response of 2.5 ($\Delta R/R_a$) to 10 ppm H₂S at an optimal temperature of 200 °C. Figure 3a,b present the band diagram of p-type CuO nanocuboids in ambient air and H₂S atmospheres, respectively. When H₂S molecules are adsorbed onto the CuO (111) plane, the ‘S’ atom can be bonded to two-fold subsurface Cu atom (Cu_{sub}) atoms through the bridge bond. However, the ‘H’ adsorbs favorably on the outermost oxygen (O_{surf}) site of the CuO lattice and displays good catalytic activity toward H₂S dissociation. A comparison of the H₂S gas-sensing performance of the pristine Cu_xO gas sensors is shown in Table 2. Different morphologies have been used for H₂S-sensing at different temperatures. However, pristine Cu_xO gas sensors show lower sensitivity compared to noble metal-decorated gas sensors or composite gas sensors. Therefore, strategies are needed to enhance the response of gas sensors toward H₂S gas.

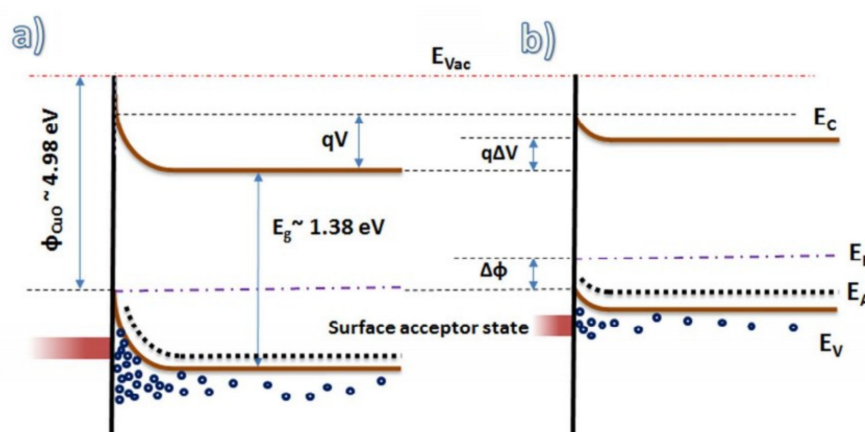


Figure 3. Energy band diagrams of CuO nanocuboid in (a) air and (b) H₂S surroundings. Reprinted from [40] with permission from ACS.

Table 2. H₂S gas-sensing properties of pristine Cu_xO-based gas sensors.

Sensor	H ₂ S Conc. (ppm)	Response (R _g /R _a)	LOD † (ppm)	Res. Time (s)/ Rec. Time (s)	T (°C)	Ref.
CuO nanoparticles	5	4.9 ± 0.43	0.2	297.5 ± 9.2/54 ± 7.1	40	[12]
CuO nanoneedles	10	76.5% (ΔR/R _a) × 100	161 ppb	92/196	150	[37]
Sea anemone-like CuO nanoarrays	5 ppb	24.08	1.52 ppb	102/539	25	[38]
CuO nanosheets	400 ppb	1.7	3 ppb	NA *	325	[39]
CuO nanocuboids	10	~2.4 (ΔR/R _a)	1	NA	200	[40]
CuO nanosheets	1	325% [(ΔR/R _a) × 100]	2 ppb	4/9	240	[41]
CuO nanowires	100 ppb	~0.2 (ΔR/R _a)	2.5 ppb	10 min/15 min	180	[42]

* NA: not available; † LOD: limit of detection; T = operating temperature

4. Pd-Decorated/Doped Cu_xO Nanostructure-Based Gas Sensors

To boost the sensing performance of metal oxide gas sensors, the addition of noble metals such as Pd, Pt, and Au has been studied extensively because of their electronic and chemical sensitization properties [43–47]. Unfortunately, there are very few studies related to the noble-metal decoration on the surface of Cu_xO nanostructures, and these are discussed below. Kim et al. [27] improved the H₂S-sensing performance of CuO nanowires (NWs) in self-heating mode through Pd decoration. They used a thermal oxidation method to grow network-like CuO NWs on a patterned interdigital electrode on a SiO₂-grown Si substrate, and subsequent Pd decoration was achieved through UV irradiation. The resulting characterizations of the pristine and Pd/CuO NWs are shown in Figure 4. Their sensing results corroborate that the sensor made of pristine CuO NWs did not show H₂S selectivity at an optimum temperature of 300 °C. However, the Pd-functionalized CuO NW sensor exhibited a higher response to H₂S at 100 °C. In addition, the pristine and Pd-loaded sensors showed responses (R_g/R_a) of 1.08 and 1.89, respectively, to 100 ppm H₂S in the self-heating mode at 5 V. The generated heat was due to the self-heating effects attributable to (i) the electron current passing through the CuO NWs, and (ii) the number of networked and directly connected CuO NWs. Because of chemical sensitization, Pd may simply dissociate and transfer oxygen molecules and target gases via the spillover effect. Consequently, higher quantities of gas molecules can reach the surface of the sensor and, accordingly, a better response is expected. In addition, some Pd can be partially converted into PdO in air. The electrons flow from CuO to Pd/PdO because of the smaller work function of CuO compared to Pd and PdO. Therefore, an HAL is formed at the CuO side. Upon reducing the gas exposure, the width of the HAL in CuO is condensed. As the initial volume/concentration of holes increases due to the presence of Pd/PdO, the reduction in

the same number of holes due to exposure to the reducing gas results in a low response of the sensor. This results in a decrease in the sensor response to the reducing gases. However, the situation is different for H₂S-sensing. CuO is transformed into CuS with metal-like conductivity upon exposure to H₂S, which results in a high resistance modulation at the heterojunctions. The height of the potential barriers decreases owing to the different work functions of CuO and CuS. This results in a higher concentration of electrons in the sensing layer (CuO/CuS) than in CuO, which decreases the concentration of holes and increases the resistance of the sensing material. In the p-type sensor, a smaller conduction volume of the hole region delivers a high sensor response.

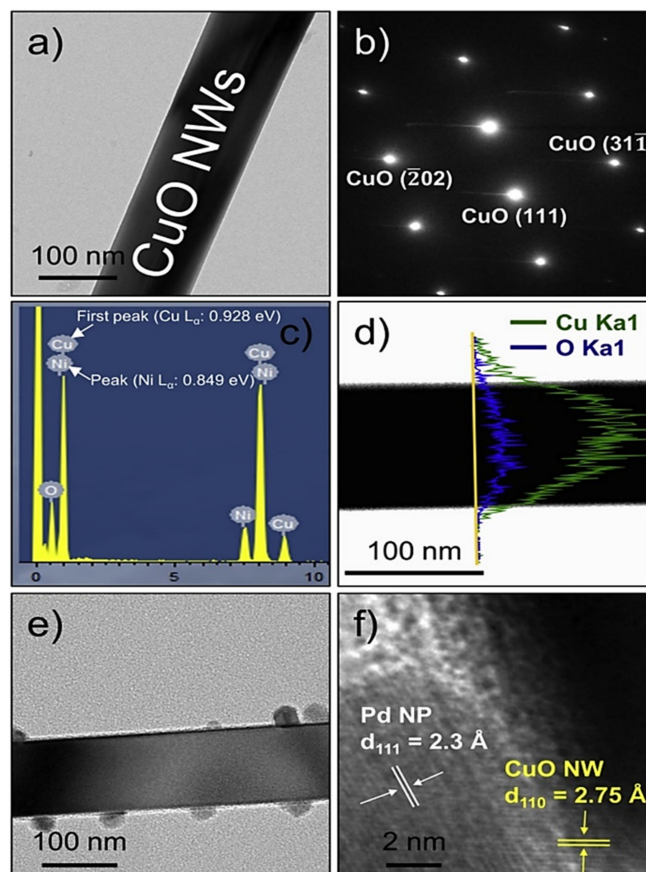
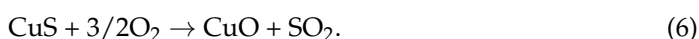
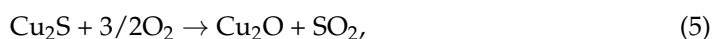


Figure 4. (a) TEM, (b) SAED, (c) EDS, and (d) EDS line profiles of CuO NW; (e) TEM and (f) HR-TEM images of Pd-loaded CuO NW. Reprinted from [27] with permission from Elsevier.

In another study, Kim et al. [48] described the development of CuO nanorods (NRs) and their respective Pd-functionalization via a three-step approach including Cu foil oxidation in air, dipping in PdCl₂, and subsequent annealing. In air, the CuO surface adsorbs oxygen from air by capturing electrons, resulting in the formation of HAL. Upon exposure to low concentrations of H₂S, the surface reactions occur spontaneously between the formerly adsorbed oxygen species and H₂S molecules; subsequently, the electrons released from the surface states recombine with the holes in the valence band, leading to an increase in the electrical resistance of the gas sensor. In contrast, at high H₂S concentrations, a layer of CuS is created on the CuO NR surface. The configuration of CuS reduces the resistance to its metallic character. In the case of Pd/CuO NRs, the adsorption and generation of free electrons through H₂S gas are advanced on the surface of Pd nanoparticles (NPs). The Pd-NPs have a larger surface area than the CuO NRs, leading to better H₂S adsorption. The H₂S molecules dissociate on the catalytic Pd-clusters and diffuse, possibly across and/or through the clusters, to the substrate, wherein H₂S gas molecules may correlate with the

CuO NRs to enhance the resistance. Therefore, through Pd loading, a higher response was observed.

Mikami et al. [49] reported the synthesis of Pd-loaded Cu₂O nanocrystals, which corroborated the H₂S responses at low concentrations (1–8 ppm) between 50 °C and 150 °C. The electrical resistance of Cu₂O was found to increase upon Pd loading because of the configuration of the Schottky junctions between Cu₂O and Pd. They noticed that the resistance of the sensor decreased abruptly for high Pd loading (5 mol.% and 10 mol.%), signifying that adding a suitable quantity of Pd to the Cu₂O nanocrystals suppresses Cu₂O sulfurization and supports the reaction of the adsorbed oxygen with H₂S. In fact, catalytic H₂S dissociation on Pd facilitated the reaction of adsorbed oxygen with H₂S gas. Upon stoppage of H₂S gas, Cu₂O and CuO oxides were formed in air according to following equations:



The standard Gibbs free energies of Equations (5) and (6) at 50 °C and 150 °C are −359.411, −372.825, −350.166, and −364.33 kJ/mol, respectively, indicating that these reactions are thermodynamically favorable at 50 and 150 °C. This demonstrates the reversible nature of gas sensors.

Lastly, Hu et al. [50] developed a Pd-doped (0–1.5 wt.%) CuO gas sensor for H₂S-sensing. The ionic radius of Cu²⁺ (0.73 Å) is smaller than that of Pd²⁺ (0.86 Å), and the replacement of Cu²⁺ through Pd²⁺ ions induced lattice growth, which was supported by the XRD pattern. Sensing studies showed that the H₂S response of the Pd-doped CuO (1.25 wt.%) sensor was 7.9 times greater than that of the pristine CuO sensor ($R_g/R_a = 15.7$) at 80 °C. The upgraded response characteristics of the Pd-doped CuO were largely ascribed to electronic sensitization. Even at room temperature, PdO has a high intrinsic carrier concentration and conductivity; thus, Pd doping can decrease the working temperature of the Pd/CuO sensor. Additionally, PdO is capable of boosting the sensing material to capture oxygen molecules and form chemisorbed oxygen atoms. In addition, due to the sensitization, PdO molecules on the surface of CuO can take part in the reactions and release electrons once they are exposed to H₂S. Accordingly, the released electrons can be recombined with holes, resulting in a reduction in the concentration of holes. Thereafter, the resistance of the Pd-doped CuO sensor increased with contact with H₂S. Compared to pristine CuO, Pd-doped CuO (1.25 wt.%) had a superior surface area and high density of adsorption sites, which resulted in excellent responses even at comparatively low H₂S concentrations. However, surface disorder occurred as the doping concentration increased to 1.50 wt.%, and it was accompanied by an increase in the density of surface states, leading to the pinning of Fermi level surfaces and, hence, a decrease in the sensor response. A list of noble-metal-decorated/doped CuO-based gas sensors for H₂S detection is presented in Table 3. As can be seen, only Pd has been used in combination with Cu_xO; in this regard, decoration/doping with other noble metals is essential. In general, Pd-decoration/doping on CuO can enhance the response of gas sensors relative to pristine gas sensors. Furthermore, it can decrease the sensing temperature and increase the stability of gas sensors [27,48–50].

Table 3. H₂S gas-sensing properties of noble metal-decorated/doped CuO-based gas sensors.

Sensing Materials	H ₂ S Conc. (ppm)	Response (R_g/R_a)	LOD (ppm)	Res. Time (s)/ Rec. Time (s)	T (°C)	Ref.
Pd-decorated CuO NWs	100	1.962	1	NA	100	[27]
Pd-decorated CuO nanorods	100	$31,243\%(\Delta R/R_a) \times 100$	20	670/80	300	[48]
Pd (1 mol.%) loaded CuO nanocrystals	8	7.9	1	NA	250	[49]
Pd-doped CuO nanoflowers	50	123.4	0.1	15/3500	80	[50]

5. Cu_xO Nanocomposite-Based Gas Sensors

An additional perspective for advancing gas-sensing performance is using heterostructures. They consist of semiconducting metal oxides of type n and p that form a p-n junction after contact [51]. Such heterojunctions generally result in a charge depletion layer among the materials, and there is a noticeable increase in the air resistance. Therefore, the release of electrons when the adsorbed oxygen comes into contact with reducing gases causes a large change in resistance, which can be beneficial for sensing applications. In the case of CuO, if a mixture of type n material and CuO is exposed to H₂S, the p-n junction may collapse because of the development of metallic CuS. Such a junction collapse is mainly related to an increase in conductivity by several orders of magnitude and the appearance of a large sensing signal [32]. In this section, we discuss the CuO-based nanocomposite heterojunctions reported for the detection of H₂S gas. The nanofiber (NF)-type structures are very promising for sensing applications [52–54]. The fabrication of metal oxide NFs can be achieved easily through a cost-effective and efficient electrospinning technique. These NFs possess larger surface areas owing to their one-dimensional morphological features. This is because they have a substantial surface area for gaseous species along with numerous nanograins and extensive grain boundary areas, which confirms the improved sensitivity of the sensors with NF-type morphology [55,56]. In an interesting study, Park et al. [57] synthesized hollow porous SnO₂-CuO NF mats using electrospinning and a thermal processing approach and applied them in H₂S sensors. The sensing mechanism was based on the development of CuS on the SnO₂-CuO surface as follows [57]:



It is well known that CuO and SnO₂ are p- and n-type semiconductor oxides, respectively. Therefore, at the interface between SnO₂ and CuO, several p-n heterojunctions with electron-depletion layers were formed upon contact. Moreover, both the inner and outer tubular structures had electron-depletion layers. When the sensor was exposed to H₂S, the p-type CuO was converted to CuS, which is a metallic material with good electrical conductivity. Ultimately, the resistance of the entire sensor of the composite was considerably reduced. Additionally, the porous morphology resulted in improved gas-surface interactions. The plausible effects of the nano-dimensional porous morphology and uniform distribution of SnO₂ to CuO interfaces, in addition to improved surface area, were attributed to the high performance of the gas sensor to H₂S gas.

Recently, metal-organic frameworks (MOFs) have been applied as materials and templates to fabricate porous micro- and nanostructures for a variety of applications [58,59]. Their advantages as templates for fabricating gas sensors are their high porosity, uniform distribution of different phases, variable composition, and controlled morphology in MOF-derived structures [60]. Furthermore, mixed metal oxides derived from MOFs can be easily obtained via a simple calcination method of these MOFs with pre-designed components. In this regard, a facile MOF-derived method was used effectively for the construction of bamboo-like CuO/In₂O₃ heterojunctions for detecting H₂S [61]. It had a large surface area of 208.13 m²/g. Furthermore, the pore sizes of pure In₂O₃ and CuO/In₂O₃ heterojunctions were 28.70 and 15.23 nm, respectively. The higher performance of the CuO/In₂O₃ heterojunction relative to pristine In₂O₃ was related to (i) the unique mesoporous structure of CuO/In₂O₃ heterostructures in which the precise interior voids and the rough surface endowed the CuO/In₂O₃ with abundant dynamic sites, remarkably enhanced the surface reactions, and resulted in a higher response compared to pristine In₂O₃, and (ii) the establishment of the p/(CuO)-n/(In₂O₃) heterojunctions and subsequent formation of a CuS layer upon exposure to H₂S gas.

WO_{3-x} is a well-known transition metal oxide that can be a promising material for sensing applications owing to the presence of oxygen vacancies [62,63]. Thus, CuO/WO_{3-x} heterojunctions were synthesized for H₂S-sensing studies. The developed heterojunction sensor exhibited an enhanced response to H₂S gas. The heterojunctions based on p-CuO x n-WO_{3-x} were formed in air; accordingly, the CuO/WO_{3-x} sensor displayed a high

baseline resistance. When the sensor was exposed to the H₂S gas, the O-S exchange reaction occurred by the collapse of the CuO/WO_{3-x} p-n junctions via the conversion of CuO to CuS, as confirmed by FTIR analysis. This resulted in a remarkable deterioration in the CuO/WO_{3-x} sensor resistance and the appearance of a sensing signal [63]. In addition, high concentrations of oxygen vacancies facilitated the adsorption of target gases, resulting in an enhancement of the response to the target gas.

In another study, Kim et al. [64] described the effect of rGO loading on the H₂S gas-sensing response of electrospun CuO NFs. It was noted that the amount of rGO strongly influenced the gas response, and the highest response was obtained with 0.5 wt.% rGO loading. The current passing via CuO was blocked when the rGO content was ≤0.5 wt.% because of the existence of discrete rGOs and the initial resistance was enhanced. Subsequently, depending on the amount of rGO, the resistance was modulated in the presence of H₂S. However, at higher rGO content (>0.1%), it offered a further pathway for current flow, which resulted in a longer conduction path along the rGO. This process reduced the initial resistance and the sensor response decreased relative to the optimal amount of rGO. The sensing mechanism in pristine CuO NFs was explained as follows: the CuO nanograins resulted in numerous CuO-CuO homojunctions, which affected the sensing behavior. As shown in Figure 5a, as oxygen penetrates the CuO grain boundaries, O₂⁻ species typically exist at grain boundaries, generating potential barriers for holes and electrons, which reduces the hole conductance across the grain boundaries and contributes to the increase in conductivity. In H₂S, CuO is transformed to CuS by sulfurization, and electrons in the CuO flow toward the CuS at the CuO/CuS hetero-interfaces, generating a potential barrier. The potential barrier width would be narrow when the grain boundary regions are transformed to CuS (Figure 5b). The potential barrier would be broad when most of the CuO is converted to CuS (Figure 5c). When the value of “b” in Figure 5b,c is larger than “a” in Figure 5a, the hole resistance can be increased further through a CuO-to-CuS transformation. However, the hole resistance decreases when “b” is smaller than “a.” In the rGO-loaded gas sensors, the electrons flow from CuO to rGO (Figure 5e) because of the difference in the work functions (Figure 5d), which results in the growth of HAL in CuO. When the rGO/CuO NF sensors were in contact with H₂S, CuO was transformed into CuS (Figure 5f,g). Upon exposure, the H₂S molecules transferred electrons to the CuO surfaces, which reduced the HAL thickness. If we assume that the rGO and CuS are in contact, then the electrons in rGO will flow to CuS, which reduces the hole accumulation, consequently increasing the hole resistance. Therefore, the H₂S exposure and the transformation of CuO to CuS unexpectedly increased the hole resistance, leading to an upgraded sensor response.

Owing to their unique electrical properties, two-dimensional (2D) layered transition metal dichalcogenides (TMDs) have gained much attention in the gas-sensing field [65,66]. As a 2D layered TMD, molybdenum disulfide (MoS₂) has exceptional properties, such as high carrier mobility, greater surface area, direct energy gap (1.8 eV), and excellent electrical properties [67]. In this context, Zhang et al. [68] synthesized CuO/MoS₂ heterojunctions for H₂S gas-sensing. The unique CuO/MoS₂ heterojunctions, made up of nanorod/nanosheet-type structures with oxygen/sulfur vacancies, had abundant dynamic sites for the adsorption of gas, which was the main cause of the excellent H₂S response of CuO/MoS₂ sensors. The main H₂S detection mechanism of the CuO/MoS₂ sensor was attributed to the p-n heterojunctions formed between p-type CuO and n-type MoS₂, leading to a higher sensor resistance in air when compared to pure CuO and MoS₂. Upon exposure of the sensing film to H₂S, CuS was formed and, owing to the excellent conductivity of metallic CuS, the p-n junction and the depletion region were destroyed, which efficiently enabled the flow of electrons and extended the conduction segment of the sensing film. The tube-like structures enable the adsorption and diffusion of target gas molecules and offer abundant active sites between the H₂S gases and chemisorbed oxygen atoms. Li et al. [69] prepared ZnO/CuO rough nanotubular arrays using a combination of ultrasonic spray pyrolysis and chemical deposition systems. The fabricated sensor showed a 61% response to 20 ppm of H₂S at 50 °C. The enhancement in the detection performance of the ZnO/CuO

structures was attributed to their distinct morphological features and p–n heterojunctions. The development of n–p junctions between the n-type ZnO and p-type CuO caused the expansion of the hole depletion layer inside the CuO, and the quantity of chemisorbed oxygen increased. Subsequently, upon H₂S gas exposure, CuS formation led to a decrease in the resistance, thereby generating a sensing signal. Furthermore, the unique tube-like architectures contain numerous tiny nanoparticles on the surface, which facilitates the rapid adsorption/diffusion of the gas molecules and results in several dynamic sites among the H₂S and adsorbed oxygen atoms. Yeh et al. [70] prepared V₂O₅ NWs decorated with CuO NPs using a chemical route for H₂S-sensing. The fabricated sensor responded to 33 to 23 ppm of H₂S gas at 225 °C. The development of p–n junctions at the CuO/V₂O₅ interfaces in conjunction with the reversible sulfuric/oxidative reactivity upon repeated H₂S gas/air exposure at reasonable temperatures remarkably boosted the selectivity and response toward H₂S [70].

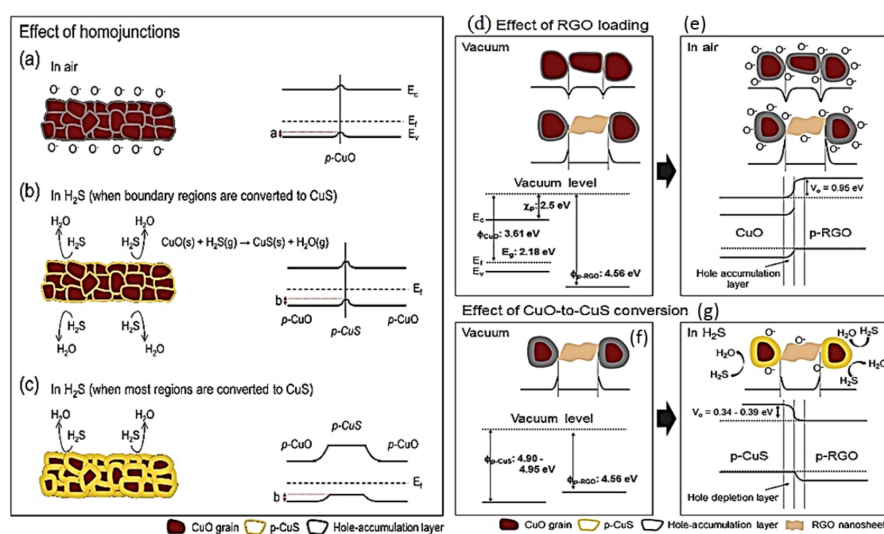


Figure 5. Effect of (a) oxygen adsorption and (b,c) conversion of CuO to CuS on the CuO/CuS band structure; (d) energy band structure CuO–rGO before contact in vacuum; (e) formation of potential barriers upon the contact of rGO–CuO in air; (f) energy band structure CuS–rGO before contact in vacuum; (g) formation of potential barriers upon the contact of rGO–CuS in H₂S gas. Reprinted from [64] with permission from Elsevier.

Commonly, gas sensors constructed with metal oxides work at higher temperatures (200–500 °C). Therefore, owing to the higher energy consumption, it is difficult to integrate them into electronic devices. Thus, room-temperature [71,72] or self-powered [73,74] gas sensors are in high demand to overcome the power consumption issues, which allows sensors to be integrated into portable devices [75].

In this respect, Kim et al. [76] developed gas sensors based on pure SnO₂ NWs, CuO-functionalized SnO₂ NWs, and CuO-functionalized SnO₂–ZnO core–shell NWs with different shell thicknesses for self-heating H₂S detection. Figure 6 shows the generated temperatures in the sensors with various shell thicknesses upon the application of different voltages. The sensing results suggested that the sensor with the thickest shell offered the highest response to H₂S, presumably due to the more prominent self-heating effect generated, as shown in the thermographs in Figure 6. In C–S NWs with a thick ZnO shell, the current flows via the ZnO shell and there are different sources of Joule heating. First, Joule heating can occur inside the ZnO grains and, therefore, the electrons flow inside these grains. Second, the ZnO grain boundaries act as an alternative source for Joule heating. Third, because of the networked character of ZnO NWs, they trace one another, and Joule heating occurs at the resultant ZnO–ZnO homojunctions (Figure 7).

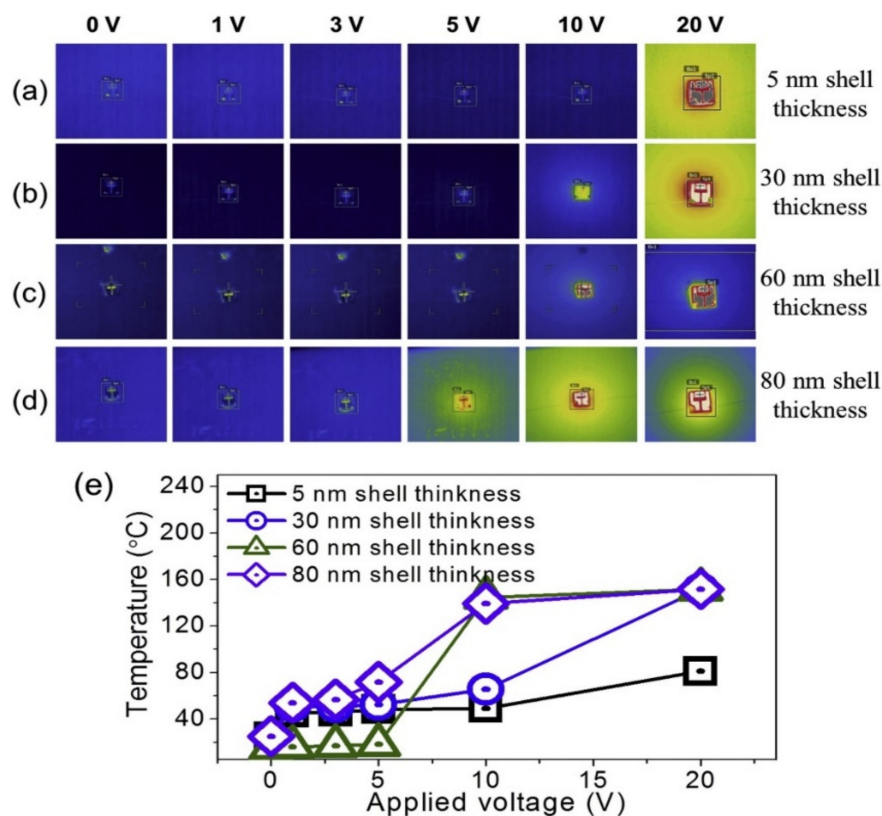


Figure 6. (a–d) Thermographs of CuO-functionalized SnO₂–ZnO core–shell NW sensors with varied shell thicknesses of 5, 30, 60, and 80 nm, respectively, at different applied voltages; (e) equivalent plot of temperature as a function of applied voltage of gas sensors. Reprinted from [76] with permission from Elsevier.

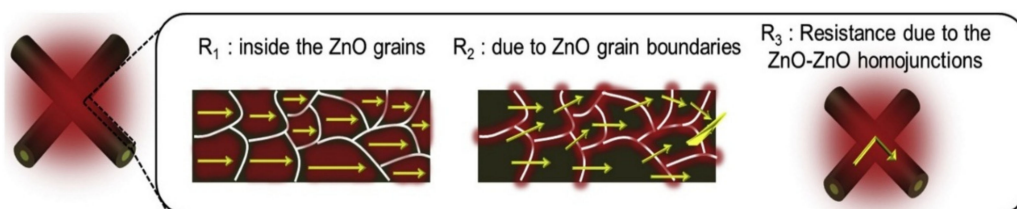


Figure 7. Effects of self-heating in SnO₂–ZnO core–shell NWs. Reprinted from [76] with permission from Elsevier.

The sensor fabricated with the thickest ZnO shell had a greater self-heating effect at a voltage of 5 V, which was because the possibilities of direct contact among the ZnO–ZnO shells were enhanced with increasing shell thickness. Several factors accounted for the sensing mechanism. First, the modulation of resistance on the ZnO or SnO₂ surface enhanced the detection activities. Second, owing to the networked nature of the synthesized products, many ZnO–ZnO homojunctions acted as sources of resistance modulation in gas sensors. Third, the generation of ZnO/SnO₂ heterojunctions due to the C–S nature of the synthesized materials and the subsequent modulation of potential barriers in the presence of H₂S affected the results. Fourth, the CuO-to-CuS transformation affected the sensing results. In the presence of H₂S, CuO reacts with H₂S to form intermetallic CuS compounds with metal-like conductivities. With a ZnO shell thickness of 80 nm in C–S NWs, although the depletion region is formed through oxygen chemisorption, the nondepleted region in the ZnO shell has substantial depth. When H₂S is introduced, the CuO was transformed into CuS and destroyed the ZnO–CuO heterojunctions, subsequently decreasing the sensor resistance. The conversion to Cu₂S also upgrades the sensing process, albeit less feasibly

than CuS. In the case of the pure SnO₂ NW sensor, a low response to H₂S was recorded because of the low self-heating in the bare SnO₂ sensor, wherein H₂S cannot attain sufficient energy for the dynamic adsorption onto the surface of the SnO₂ NWs.

Kim et al. [77] investigated the effect of CuO coverage on the surface of ZnO nanorods. They prepared CuO/ZnO nanorods using a combination of hydrothermal and photochemical methods. The p–n heterojunctions generated between ZnO and CuO in air and their subsequent destruction by the conversion of CuO to CuS in the presence of H₂S were the main reasons for the enhanced response to H₂S relative to the pristine CuO gas sensor. The sensing results demonstrated that the response of H₂S improved with an increase in the CuO coverage up to a 0.05 μ M Cu salt concentration. In the presence of H₂S, the spike-shaped CuO transformed into a wide and flat-shaped Cu₂S, which was more prevalent with higher CuO coverage. The wide and flat Cu₂S structures condensed the dynamic sensing area of the ZnO nanorods and impeded the target gas detection on the surface. Furthermore, excessive CuO coverage on the ZnO nanorods resulted in the partial transformation of CuO to metallic Cu₂S and resulted in a substantial quantity of unreacted CuO. Park et al. [78] utilized a solvothermal route for the synthesis of nanoparticles based on CuO-ZnO composites (CuO:ZnO = 4:1 by vol.%). It showed an enhanced response to H₂S compared to pristine gas sensors. The CuO-ZnO sensor had both p–n CuO/ZnO heterojunctions and p–p CuO/CuO homojunctions. The sensing mechanism is shown in Figure 8.

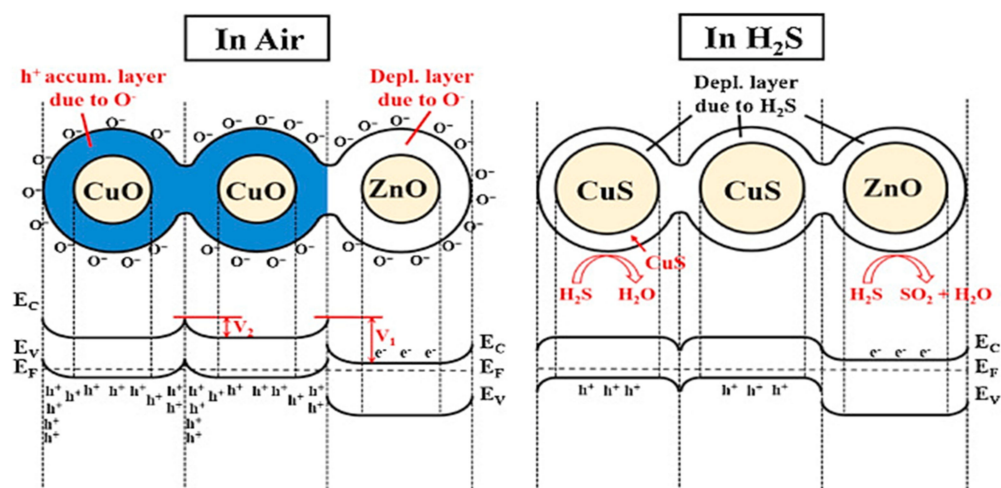


Figure 8. Schematic of energy levels in CuO-ZnO heterojunctions in air and H₂S gas. Reprinted from [78] with permission from Elsevier.

In ambient air, an electron depletion layer was formed on the ZnO side while the HAL was on the CuO side of the p-CuO/n-ZnO heterojunction. The potential energy barrier V_1 at the CuO-ZnO interface was greater than that of V_2 at the CuO-CuO interface. In the H₂S atmosphere, the reverse scenario occurred wherein the depletion layers were produced on both the CuO and ZnO sides. In such a case, the holes could not transfer from p-CuO to n-ZnO as they were blocked by the internal fields. Therefore, the electrical resistance increased remarkably, which caused the generation of resistance modulation and a high response to H₂S.

Wang et al. [79] synthesized 1D α -MoO₃/CuO nanocomposites using a simple method. The developed sensor exhibited improved H₂S-sensing features, such as a lower working temperature, high response, and good selectivity. The different work functions created p–n junction barriers at the interfaces between the two materials. The width of the p–n barrier junctions was equivalent to the dimensions of the CuO NPs because of their small diameters. Initially, the resistance was high in ambient air, and CuO was transformed into CuS in an H₂S atmosphere. Thereafter, the height/width of the p–n junction barriers

reduced or the barriers disappeared, depending on the H_2S concentration and working temperature. At low temperatures, the rate of conversion between CuS and CuO was slow. Therefore, the response/recovery times of the sensor at lower temperatures ($<80^\circ\text{C}$) were greater than those at higher temperatures. The good selectivity to H_2S gas was evidenced by the fact that the p–n junctions did not disappear as the sensor was exposed to other gases. The well-dispersed semiconducting powders offer better surface areas for gas-detecting reactions. However, owing to the strong van der Waals attraction, the formation of hard aggregation among the core particles is difficult to avoid.

Compared to their powder counterparts, nanostructures based on quasi-one-dimensional oxides with reduced agglomeration are beneficial to the uniform addition of functionalizing elements and quick diffusion of gas toward the sensing surface [80–83]. In this regard, Hwang et al. [84] prepared CuO -functionalized SnO_2 NW gas sensors by depositing a slurry containing SnO_2 NWs on a polydimethylsiloxane (PDMS)-guided substrate followed by dropping an aqueous Cu nitrate solution. The selective detection of H_2S in addition to the enhanced rapid gas response was attributed to the uniform CuO distribution on the surface of the less-agglomerated network of SnO_2 NWs. Disruption of the resistive CuO/SnO_2 p–n heterojunction structures through the sulfurization of CuO into a highly conducting CuS phase acted as the main detection mechanism, and the development of a conducting heterostructure based on $\text{CuS}/\text{n-SnO}_2$ was responsible for the selective detection of H_2S . In another similar study, Shao et al. [85] prepared p- CuO (particle)/n- SnO_2 NW heterostructures for H_2S gas-sensing studies, and the same sensing mechanism was proposed for H_2S detection, as shown in Figure 9.

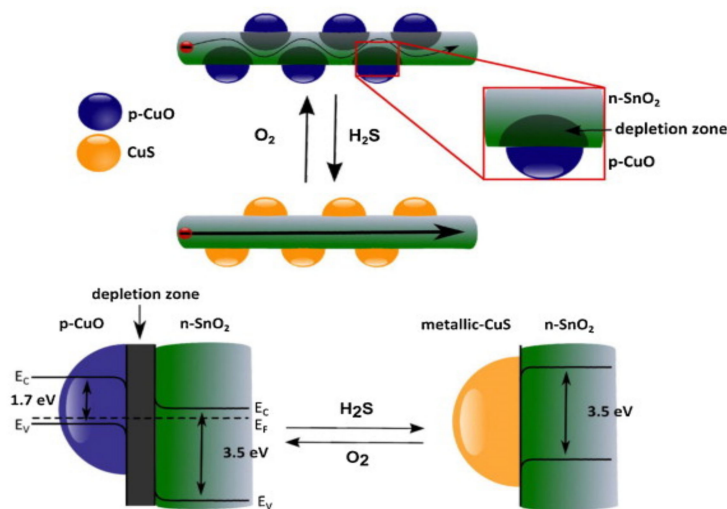


Figure 9. Sensing mechanism of CuO-SnO_2 heterojunctions. Reprinted from [85] with permission from Elsevier.

Despite the research reported thus far on CuO -loaded SnO_2 , there are relatively fewer reports that describe the humidity dependence of SnO_2 gas sensors through CuO loadings. Choi et al. [86] used the ultrasonic spray pyrolysis approach to develop CuO -loaded SnO_2 hollow spheres and examined their H_2S -sensing properties under dry and humid conditions. The developed CuO -loaded SnO_2 sensor displayed n-type gas-sensing features, which signified that conduction occurred in the CuO -loaded sensor along the n- SnO_2 hollow spheres. The air resistance was increased by three orders of magnitude due to the development of resistive-type nanoscale p–n junctions between CuO and SnO_2 . The authors revealed that the interactions between the water molecules and CuO nanoclusters were the main cause underlying the validation of contacts between humidity and SnO_2 .

Ramgir et al. [87] developed randomly distributed nano p–n heterojunctions based on CuO and WO_3 for the detection of H_2S . The p–n nanojunctions developed at the grain boundary between CuO and WO_3 were caused by the formation of a potential barrier.

Upon H₂S exposure, the H₂S gas molecules interact with the adsorbed oxygen species and consequently release a large number of free electrons.

In the case of n-WO₃ and p-CuO, the release of electrons resulted in a decrease and increase in the sensor resistance, respectively. However, at the interface of WO₃/CuO (at a high temperature of 300 °C), H₂S molecules interacted with CuO to form CuS. The formation of metallic CuS led to the collapse of the barrier, which led to the release of electrons in the WO₃ matrix and the appearance of a sensing signal (Figure 10).

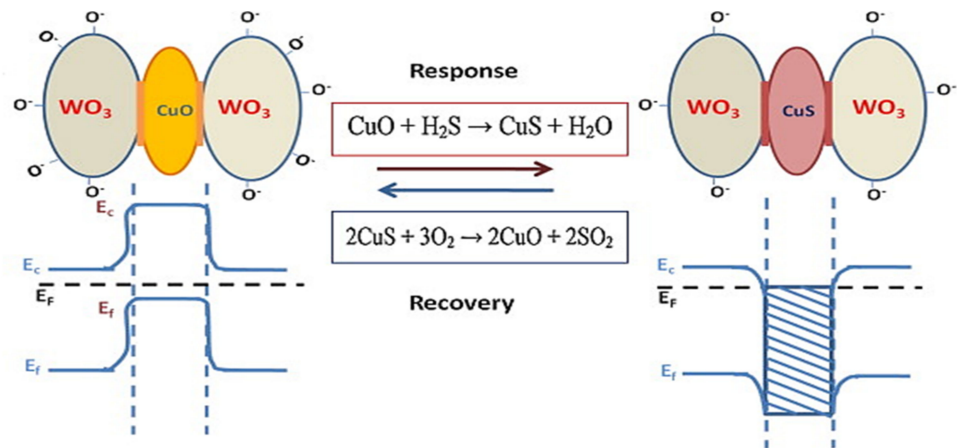


Figure 10. Schematic of the H₂S-sensing mechanism in CuO/WO₃ heterojunctions. Reprinted from [87] with permission from Elsevier.

A recorded work function area map for pristine and CuO-modified WO₃ films (Cu: 2.25%) is presented in Figure 11a. The observed average values of the work function for pristine and CuO-modified WO₃ were 5.032 and 5.208 eV, respectively. Figure 11b shows that work functions increase with respect to the CuO content, which enhances p–n junction formation over the sensor film surface. A reduction in the work function of the CuO-modified WO₃ sensor (~0.2 eV) upon H₂S exposure was observed (Figure 12), which was attributed to the unique interactions of CuO with H₂S, resulting in the development of CuS.

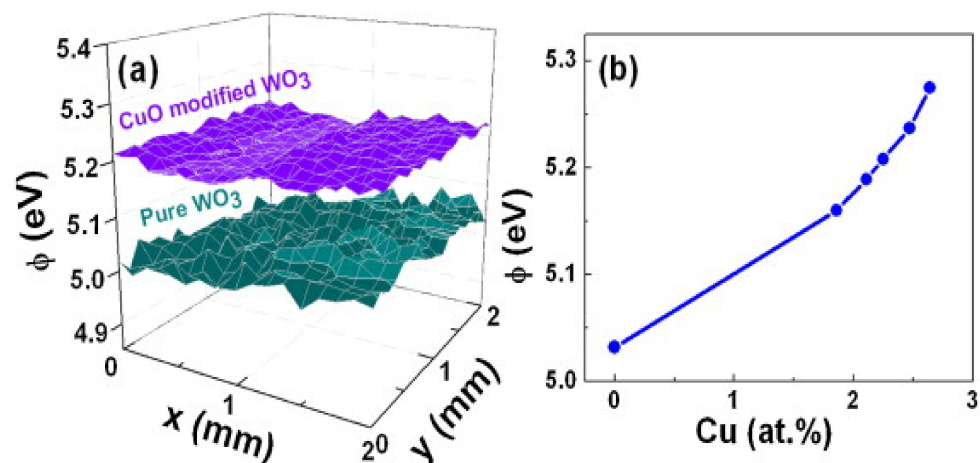


Figure 11. (a) Work function area maps of pristine and CuO-modified WO₃ films; (b) plot of change in work function vs. Cu (at.%). Reprinted from [87] with permission from Elsevier.

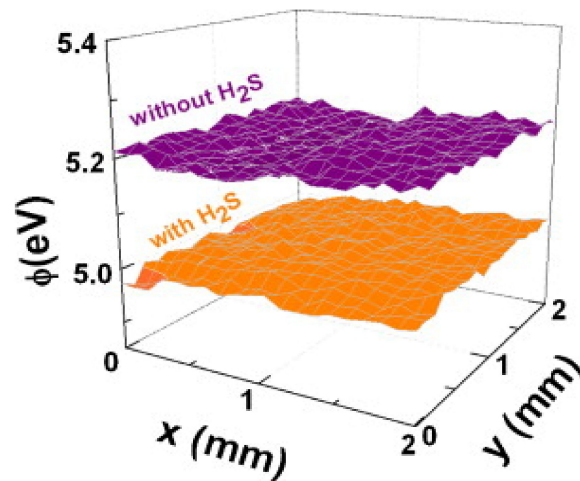


Figure 12. Change in work function of CuO-modified WO₃ films in the presence of 50 ppm H₂S. Reprinted from [87] with permission from Elsevier.

The H₂S gas-sensing performances of the CuO-based composite heterojunction sensors are summarized in Table 4, wherein different gas sensors with various morphologies were used for the detection of H₂S at different temperatures.

Table 4. H₂S gas-sensing performances of CuO-based sensors.

Sensing Materials	H ₂ S Conc. (ppm)	Response (R _g /R _a)	LOD	Res. Time (s)/ Rec. Time (s)	Tempt. (°C)	Ref.
SnO ₂ -CuO nanotubes	5	1395 (R _a /R _g)	1	5.27/NA	200	[57]
Bamboo-like CuO/In ₂ O ₃ (3.5 wt.%) heterostructure	5	229.3	200 ppb	10/3600	70	[61]
rGO-loaded CuO NFs	10	11.7	1	NA	300	[64]
CuO-MoS ₂	30	61% (R _a - R _g /R _a × 100)	1 ppb	26/18	25	[68]
ZnO/CuO nanotubes	20	42% [(R _g - R _a /R _a) × 100]	1	37/94	50	[69]
CuO/V ₂ O ₅ hybrid nanowires	23	31.86	7	130/218	220	[70]
CuO-functionalized SnO ₂ -ZnO core-shell NWs	10	2.5	1	NA	50 (5 V)	[76]
CuO/ZnO nanorods	50	~890 [(I _g - I _a)/I _a]	6.75	~900/NA	500	[77]
CuO-ZnO composite	2	1035% [(R _g /R _a) × 100]	0.1	30/98	225	[78]
MoO ₃ -CuO nanocomposite	5	7.9 (R _a /R _g)	5	NA	100	[79]
CuO-functionalized SnO ₂ NWs	20	809	20	1/332	300	[84]
CuO-loaded SnO ₂ hollow spheres	1	3.14 (R _a /R _g)	0.2	NA	300/80%RH	[86]
CuO-modified WO ₃	10	534 (R _a /R _g)	2	5/24 min	300	[87]
ZnO/CuO nanocomposite	10	393.35	300 ppb	173/NA	40	[88]
CuO/NiO nanowall arrays	5	36.9	0.5 ppb	13/60	133	[89]
CuO-SnO ₂ NFs	50	23.58 (R _a /R _g)	1	105/152	180	[90]
CNTs/SnO ₂ /CuO composites	40	19% (ΔR/R _a) × 100	10	4 min/10 min	25	[91]

6. Comparison of Different CuO-Based Gas Sensors

Different researchers have reported various mechanisms for H₂S-sensing by CuO-based gas sensors. However, the most accepted mechanism is conversion of CuO to CuS upon exposure of gas sensor to H₂S gas. This has been demonstrated by work function measurements [87] and XPS studies [39]. For pristine gas sensors, this could result in a

higher response and accordingly a higher selectivity toward H₂S gas. However, since only resistance modulation takes place on the outer surfaces of the gas sensor, no significant sensing enhancement can be resulted. In contrast, for composite or heterojunction gas sensors, especially for p-CuO/n-metal oxide heterojunctions, heterojunctions are initially formed in air and, after exposure to H₂S, formation of CuS can destroy heterojunctions, thereby significantly modulating the sensor resistance. Thus, a higher response is expected for composite gas sensors. For Pd-decorated gas sensors, an enhancement of sensor dynamics such as response time and recovery time, as well as a decrease in sensing temperature, can be obtained. Furthermore, due to the catalytic activity of Pd, a higher response relative to pristine gas sensors is expected.

From sensitivity and selectivity points of view, the sensors loaded with Pd NPs, as well as composite gas sensors, have higher sensitivity and selectivity to H₂S due to conversion of CuO to CuS with higher metallic conductivity and larger change in electrical resistance. Regarding stability of gas sensors, since pristine gas sensors generally work at high temperatures, their stability may be lower relative to Pd-loaded or composites that generally work at lower temperatures. Repeatability of metal oxide gas sensors is often good; however, regarding CuO, due to conversion to CuS, the repeatability depends on the recovery period and, in some cases, especially for pristine gas sensors due to slower sensor dynamics, repeatability is not as good as Pd-decorated or composite gas sensors.

Overall, a combination of Pd decoration on the surface of CuO-based composites can be a good strategy for realization of high-performance H₂S gas sensors. With such a composition and design, it is expected that not only response and selectivity would increase, but also sensor dynamics could be faster. However, there are a few papers working on ternary compositions for H₂S-sensing.

7. Conclusions

In this review, we discussed the H₂S gas sensor properties of Cu_xO-based gas sensors in resistive-based mode. Different forms of Cu_xO, namely, the pristine form, composite form, and noble metal-decorated/doped form, are discussed. Pristine gas sensors exhibit relatively lower responses and high sensing temperatures. However, using composites, it is possible to enhance the gas-sensing response and sensing temperature. Decoration/loading of noble metals is an additional approach to boost the response sensors toward H₂S gas due to the catalytic activities of noble metals. However, to the best of our knowledge, only Pd is used for the decoration/doping of CuO-based gas sensors for H₂S detection; Pt and Au doping merits further study. The advantage of Cu_xO-based gas sensors for H₂S gas-sensing is the selective detection of H₂S due to the conversion of Cu_xO to Cu_xS, which has high metallic conductivity. Thus, by carefully manipulating the morphology, chemical composition, and sensing temperature, it is possible to construct high-performance H₂S gas sensors with good selectivity.

Author Contributions: Conceptualization, A.M., H.W.K. and S.S.K.; writing—original draft preparation, A.M. and M.S.; writing—review and editing, A.M., M.S., S.N. and S.M.M.; supervision, H.W.K. and S.S.K.; funding acquisition, S.S.K. All authors have read and agreed to the published version of the manuscript.

Funding: This work was supported by a National Research Foundation of Korea (NRF) grant funded by the Korea government (MSIT) (No. 2021R1A2C1009790).

Institutional Review Board Statement: Not applicable.

Informed Consent Statement: Not applicable.

Data Availability Statement: Not applicable.

Acknowledgments: Authors are pleased to acknowledge Inha University for the support.

Conflicts of Interest: The authors declare no conflict of interest.

References

1. Hu, Y.; Li, L.; Zhang, L.; Lv, Y. Dielectric barrier discharge plasma-assisted fabrication of g-C₃N₄-Mn₃O₄ composite for high-performance cataluminescence H₂S gas sensor. *Sens. Actuators B Chem.* **2017**, *239*, 1177–1184. [[CrossRef](#)]
2. Li, H.; Liu, T.; Su, S.; Jin, M.; Fang, W.; Liu, L.; Wang, Y.; Hu, S.; Xiang, J. Effect of Ce modification on desulfurization performance of regenerated sorbent for high temperature H₂S removal from coal gas. *Fuel* **2021**, *293*, 120463. [[CrossRef](#)]
3. Abdel Rahman, N.S.; Greish, Y.E.; Mahmoud, S.T.; Qamhieh, N.N.; El-Maghraby, H.F.; Zeze, D. Fabrication and characterization of cellulose acetate-based nanofibers and nanofilms for H₂S gas sensing application. *Carbohydr. Polym.* **2021**, *258*, 117643. [[CrossRef](#)]
4. Mirzaei, A.; Kim, S.S.; Kim, H.W. Resistance-based H₂S gas sensors using metal oxide nanostructures: A review of recent advances. *J. Hazard. Mater.* **2018**, *357*, 314–331. [[CrossRef](#)] [[PubMed](#)]
5. Zheng, D.; Jiang, Z.; Shi, J.; Wang, Y.; Liu, Z. Experimental analysis of the effect of nitrogen gas on the H₂S stripping process during the pigging operation of a long crude oil pipeline. *Case Stud. Therm. Eng.* **2020**, *22*, 100741. [[CrossRef](#)]
6. Hoa, T.T.N.; Le, D.T.T.; Van Toan, N.; Van Duy, N.; Hung, C.M.; Van Hieu, N.; Hoa, N.D. Highly selective H₂S gas sensor based on WO₃-coated SnO₂ nanowires. *Mater. Today Commun.* **2021**, *26*, 102094. [[CrossRef](#)]
7. Ho, D.M.; Ho, B.Q.; Le, T.V. Evaluate of air pollution dispersion and propose planning scenarios to reduce air pollution for livestock activities in Tan Thanh district, Ba Ria—Vung Tau province. *Sci. Technol. Dev. J. Sci. Earth Environ.* **2019**, *2*, 26–37. [[CrossRef](#)]
8. Asad, M.; Sheikhi, M.H.; Pourfath, M.; Moradi, M. High sensitive and selective flexible H₂S gas sensors based on Cu nanoparticle decorated SWCNTs. *Sens. Actuators B Chem.* **2015**, *210*, 1–8. [[CrossRef](#)]
9. Padua, L.M.G.; Yeh, J.-M.; Santiago, K.S. A Novel Application of Electroactive Polyimide Doped with Gold Nanoparticles: As a Chemiresistor Sensor for Hydrogen Sulfide Gas. *Polymers* **2019**, *11*, 1918. [[CrossRef](#)]
10. Somacescu, S.; Stanoiu, A.; Dinu, I.V.; Calderon-Moreno, J.M.; Florea, O.G.; Florea, M.; Osiceanu, P.; Simion, C.E. CuWO₄ with CuO and Cu(OH)₂ native surface layers for H₂S detection under in-field conditions. *Materials* **2021**, *14*, 465. [[CrossRef](#)]
11. Hsu, K.-C.; Fang, T.-H.; Hsiao, Y.-J.; Li, Z.-J. Rapid detection of low concentrations of H₂S using CuO-doped ZnO nanofibers. *J. Alloy. Compd.* **2021**, *852*, 157014. [[CrossRef](#)]
12. Peng, F.; Sun, Y.; Lu, Y.; Yu, W.; Ge, M.; Shi, J.; Cong, R.; Hao, J.; Dai, N. Studies on Sensing Properties and Mechanism of CuO Nanoparticles to H₂S Gas. *Nanomaterials* **2020**, *10*, 774. [[CrossRef](#)] [[PubMed](#)]
13. Ali, F.I.M.; Mahmoud, S.T.; Awwad, F.; Greish, Y.E.; Abu-Hani, A.F.S. Low power consumption and fast response H₂S gas sensor based on a chitosan-CuO hybrid nanocomposite thin film. *Carbohydr. Polym.* **2020**, *236*, 116064. [[CrossRef](#)] [[PubMed](#)]
14. Hittini, W.; Abu-Hani, A.F.; Reddy, N.; Mahmoud, S.T. Cellulose-Copper Oxide hybrid nanocomposites membranes for H₂S gas detection at low temperatures. *Sci. Rep.* **2020**, *10*, 1–9. [[CrossRef](#)]
15. Pravarthana, N.D.; Tyagi, A.; Jagadale, T.C.; Prellier, W.; Aswal, D.K. Highly sensitive and selective H₂S gas sensor based on TiO₂ thin films. *Appl. Surf. Sci.* **2021**, *549*, 149281. [[CrossRef](#)]
16. Mokoena, T.P.; Tshabalala, Z.P.; Hillie, K.T.; Swart, H.C.; Motaung, D.E. The blue luminescence of p-type NiO nanostructured material induced by defects: H₂S gas sensing characteristics at a relatively low operating temperature. *Appl. Surf. Sci.* **2020**, *525*, 146002. [[CrossRef](#)]
17. Tang, Y.; Wu, W.; Wang, B.; Dai, X.; Xie, W.; Yang, Y.; Zhang, R.; Shi, X.; Zhu, H.; Luo, J.; et al. H₂S gas sensing performance and mechanisms using CuO-Al₂O₃ composite films based on both surface acoustic wave and chemiresistor techniques. *Sens. Actuators B Chem.* **2020**, *325*, 128742. [[CrossRef](#)]
18. Wu, Y.-Y.; Song, B.-Y.; Zhang, X.-F.; Deng, Z.-P.; Huo, L.-H.; Gao, S. Microtubular α-Fe₂O₃/Fe₂(MoO₄)₃ heterostructure derived from absorbent cotton for enhanced ppb-level H₂S gas-sensing performance. *J. Alloy. Compd.* **2021**, *867*, 158994. [[CrossRef](#)]
19. El-Shamy, A.G. New nano-composite based on carbon dots (CDots) decorated magnesium oxide (MgO) nanoparticles (CDots@MgO) sensor for high H₂S gas sensitivity performance. *Sens. Actuators B Chem.* **2021**, *329*, 129154. [[CrossRef](#)]
20. Yang, D.; Chen, G.; Fu, J.; Zhu, Y.; Dai, Z.; Wu, L.; Liu, J. The mitigation performance of ventilation on the accident consequences of H₂S-containing natural gas release. *Process Saf. Environ. Prot.* **2021**, *148*, 1327–1336. [[CrossRef](#)]
21. Yang, S.; Sun, J.; Xu, L.; Zhou, Q.; Chen, X.; Zhu, S.; Dong, B.; Lu, G.; Song, H. Au@ZnO functionalized three-dimensional macroporous WO₃: A application of selective H₂S gas sensor for exhaled breath biomarker detection. *Sens. Actuators B Chem.* **2020**, *324*, 128725. [[CrossRef](#)]
22. Song, B.-Y.; Zhang, M.; Teng, Y.; Zhang, X.-F.; Deng, Z.-P.; Huo, L.-H.; Gao, S. Highly selective ppb-level H₂S sensor for spendable detection of exhaled biomarker and pork freshness at low temperature: Mesoporous SnO₂ hierarchical architectures derived from waste scallion root. *Sens. Actuators B Chem.* **2020**, *307*, 127662. [[CrossRef](#)]
23. Pandey, S.K.; Kim, K.-H.; Tang, K.-T. A review of sensor-based methods for monitoring hydrogen sulfide. *TrAC Trends Anal. Chem.* **2012**, *32*, 87–99. [[CrossRef](#)]
24. Vuong, N.M.; Chinh, N.D.; Huy, B.T.; Lee, Y.-I. CuO-Decorated ZnO hierarchical nanostructures as efficient and established sensing materials for H₂S gas sensors. *Sci. Rep.* **2016**, *6*, 26736. [[CrossRef](#)]
25. Ali, F.I.M.; Awwad, F.; Greish, Y.E.; Mahmoud, S.T. Hydrogen Sulfide (H₂S) Gas Sensor: A Review. *IEEE Sens. J.* **2019**, *19*, 2394–2407. [[CrossRef](#)]
26. Peng, F.; Sun, Y.; Yu, W.; Lu, Y.; Hao, J.; Cong, R.; Shi, J.; Ge, M.; Dai, N. Gas sensing performance and mechanism of CuO(p)-WO₃(n) composites to H₂S gas. *Nanomaterials* **2020**, *10*, 1162. [[CrossRef](#)] [[PubMed](#)]

27. Kim, J.-Y.; Lee, J.-H.; Kim, J.-H.; Mirzaei, A.; Kim, H.W.; Kim, S.S. Realization of H₂S sensing by Pd-functionalized networked CuO nanowires in self-heating mode. *Sens. Actuators B Chem.* **2019**, *299*, 126965. [[CrossRef](#)]
28. Mirzaei, A.; Leonardi, S.G.; Neri, G. Detection of hazardous volatile organic compounds (VOCs) by metal oxide nanostructures-based gas sensors: A review. *Ceram. Int.* **2016**, *42*, 15119–15141. [[CrossRef](#)]
29. Mirzaei, A.; Neri, G. Microwave-assisted synthesis of metal oxide nanostructures for gas sensing application: A review. *Sens. Actuators B Chem.* **2016**, *237*, 749–775. [[CrossRef](#)]
30. Nasri, A.; Pétrissans, M.; Fierro, V.; Celzard, A. Gas sensing based on organic composite materials: Review of sensor types, progresses and challenges. *Mater. Sci. Semicond. Process.* **2021**, *128*, 105744. [[CrossRef](#)]
31. Ayesh, A.I.; Abu-Hani, A.F.; Mahmoud, S.T.; Haik, Y. Selective H₂S sensor based on CuO nanoparticles embedded in organic membranes. *Sens. Actuators B Chem.* **2016**, *231*, 593–600. [[CrossRef](#)]
32. Boepple, M.; Zhu, Z.; Hu, X.; Weimar, U.; Barsan, N. Impact of heterostructures on hydrogen sulfide sensing: Example of core-shell CuO/CuFe₂O₄ nanostructures. *Sens. Actuators B Chem.* **2020**, *321*, 128523. [[CrossRef](#)]
33. Nadargi, D.Y.; Tamboli, M.S.; Patil, S.S.; Dateer, R.B.; Mulla, I.S.; Choi, H.; Suryavanshi, S.S. Microwave-Epoxy-Assisted Hydrothermal Synthesis of the CuO/ZnO Heterojunction: A Highly Versatile Route to Develop H₂S Gas Sensors. *ACS Omega* **2020**, *5*, 8587–8595. [[CrossRef](#)]
34. Paul, A.; Weinberger, C.; Tiemann, M.; Wagner, T. Copper Oxide/Silica Nanocomposites for Selective and Stable H₂S Gas Detection. *ACS Appl. Nano Mater.* **2019**, *2*, 3335–3338. [[CrossRef](#)]
35. Balsamo, M.; Cimino, S.; de Falco, G.; Erto, A.; Lisi, L. ZnO-CuO supported on activated carbon for H₂S removal at room temperature. *Chem. Eng. J.* **2016**, *304*, 399–407. [[CrossRef](#)]
36. Van Toan, N.; Hung, C.M.; Hoa, N.D.; Van Duy, N.; Le, D.T.T.; Viet, N.N.; Phuoc, P.H.; Van Hieu, N. Enhanced NH₃ and H₂ gas sensing with H₂S gas interference using multilayer SnO₂/Pt/WO₃ nanofilms. *J. Hazard. Mater.* **2021**, *412*, 125181. [[CrossRef](#)] [[PubMed](#)]
37. Hu, Q.; Zhang, W.; Wang, X.; Wang, Q.; Huang, B.; Li, Y.; Hua, X.; Liu, G.; Li, B.; Zhou, J.; et al. Binder-free CuO nanoneedle arrays based tube-type sensor for H₂S gas sensing. *Sens. Actuators B Chem.* **2021**, *326*, 128993. [[CrossRef](#)]
38. Huang, Z.; Wang, X.; Sun, F.; Fan, C.; Sun, Y.; Jia, F.; Yin, G.; Zhou, T.; Liu, B. Super response and selectivity to H₂S at room temperature based on CuO nanomaterials prepared by seed-induced hydrothermal growth. *Mater. Des.* **2021**, *201*, 109507. [[CrossRef](#)]
39. Miao, J.; Chen, C.; Lin, J.Y. Humidity independent hydrogen sulfide sensing response achieved with monolayer film of CuO nanosheets. *Sens. Actuators B Chem.* **2020**, *309*, 127785. [[CrossRef](#)]
40. Dhakshinamoorthy, J.; Pullithadathil, B. New Insights Towards Electron Transport Mechanism of Highly Efficient p-Type CuO (111) Nanocuboids-Based H₂S Gas Sensor. *J. Phys. Chem. C* **2016**, *120*, 4087–4096. [[CrossRef](#)]
41. Zhang, F.; Zhu, A.; Luo, Y.; Tian, Y.; Yang, J.; Qin, Y. CuO Nanosheets for Sensitive and Selective Determination of H₂S with High Recovery Ability. *J. Phys. Chem. C* **2010**, *114*, 19214–19219. [[CrossRef](#)]
42. Li, X.; Wang, Y.; Lei, Y.; Gu, Z. Highly sensitive H₂S sensor based on template-synthesized CuO nanowires. *RSC Adv.* **2012**, *2*, 2302–2307. [[CrossRef](#)]
43. Hosseini, Z.S.; Mortezaali, A.; Iraj, A.; Fardindoost, S. Sensitive and selective room temperature H₂S gas sensor based on Au sensitized vertical ZnO nanorods with flower-like structures. *J. Alloy. Compd.* **2015**, *628*, 222–229. [[CrossRef](#)]
44. Zhou, Q.; Xu, L.; Umar, A.; Chen, W.; Kumar, R. Pt nanoparticles decorated SnO₂ nanoneedles for efficient CO gas sensing applications. *Sens. Actuators B Chem.* **2018**, *256*, 656–664. [[CrossRef](#)]
45. Ngoc, T.M.; Van Duy, N.; Hung, C.M.; Hoa, N.D.; Nguyen, H.; Tonezzer, M.; Van Hieu, N. Self-heated Ag-decorated SnO₂ nanowires with low power consumption used as a predictive virtual multisensor for H₂S-selective sensing. *Anal. Chim. Acta* **2019**, *1069*, 108–116. [[CrossRef](#)]
46. Sarica, N.; Alev, O.; Arslan, L.C.; Öztürk, Z.Z. Characterization and gas sensing performances of noble metals decorated CuO nanorods. *Thin Solid Films* **2019**, *685*, 321–328. [[CrossRef](#)]
47. Rydosz, A.; Maziarz, W.; Pisarkiewicz, T.; Wincza, K.; Gruszczyński, S. Nano-thin CuO films doped with Au and Pd for gas sensors applications. In Proceedings of the International Conference on Informatics, Electronics & Vision, Dhaka, Bangladesh, 17–18 May 2013; pp. 1–5.
48. Kim, H.; Jin, C.; Park, S.; Kim, S.; Lee, C. H₂S gas sensing properties of bare and Pd-functionalized CuO nanorods. *Sens. Actuators B Chem.* **2012**, *161*, 594–599. [[CrossRef](#)]
49. Mikami, K.; Kido, Y.; Akaishi, Y.; Quitain, A.; Kida, T. Synthesis of Cu₂O/CuO nanocrystals and their application to H₂S sensing. *Sensors* **2019**, *19*, 211. [[CrossRef](#)]
50. Hu, X.; Zhu, Z.; Chen, C.; Wen, T.; Zhao, X.; Xie, L. Highly sensitive H₂S gas sensors based on Pd-doped CuO nanoflowers with low operating temperature. *Sens. Actuators B Chem.* **2017**, *253*, 809–817. [[CrossRef](#)]
51. Miller, D.R.; Akbar, S.A.; Morris, P.A. Nanoscale metal oxide-based heterojunctions for gas sensing: A review. *Sens. Actuators B Chem.* **2014**, *204*, 250–272. [[CrossRef](#)]
52. Majhi, S.M.; Mirzaei, A.; Kim, H.W.; Kim, S.S. Reduced graphene oxide (rGO)-loaded metal-oxide nanofiber gas sensors: An overview. *Sensors* **2021**, *21*, 1352. [[CrossRef](#)] [[PubMed](#)]
53. Liu, Y.; Hao, M.; Chen, Z.; Liu, L.; Liu, Y.; Yang, W.; Ramakrishna, S. A review on recent advances in application of electrospun nanofiber materials as biosensors. *Curr. Opin. Biomed. Eng.* **2020**, *13*, 174–189. [[CrossRef](#)]

54. Mercante, L.A.; Andre, R.D.S.; Mattoso, L.H.C.; Correa, D.S. Electrospun Ceramic Nanofibers and Hybrid-Nanofiber Composites for Gas Sensing. *ACS Appl. Nano Mater.* **2019**, *2*, 4026–4042. [[CrossRef](#)]
55. Choi, S.-W.; Park, J.Y.; Kim, S.S. Growth behavior of nanograins in NiO fibers. *Mater. Chem. Phys.* **2011**, *127*, 16–20. [[CrossRef](#)]
56. Abideen, Z.U.; Katoch, A.; Kim, J.-H.; Kwon, Y.J.; Kim, H.W.; Kim, S.S. Excellent gas detection of ZnO nanofibers by loading with reduced graphene oxide nanosheets. *Sens. Actuators B Chem.* **2015**, *221*, 1499–1507. [[CrossRef](#)]
57. Park, K.-R.; Cho, H.-B.; Lee, J.; Song, Y.; Kim, W.-B.; Choa, Y.-H. Design of highly porous SnO₂-CuO nanotubes for enhancing H₂S gas sensor performance. *Sens. Actuators B Chem.* **2020**, *302*, 127179. [[CrossRef](#)]
58. Koo, W.-T.; Jang, J.-S.; Kim, I.-D. Metal-Organic Frameworks for Chemiresistive Sensors. *Chem. Eng. J.* **2019**, *5*, 1938–1963. [[CrossRef](#)]
59. Xu, K.; Zhao, W.; Yu, X.; Duan, S.; Zeng, W. MOF-derived Co₃O₄/Fe₂O₃ pn hollow cubes for improved acetone sensing characteristics. *Phys. E Low Dimens. Syst. Nanostruct.* **2020**, *118*, 113869. [[CrossRef](#)]
60. Wang, X.-F.; Song, X.-Z.; Sun, K.-M.; Cheng, L.; Ma, W. MOFs-derived porous nanomaterials for gas sensing. *Polyhedron* **2018**, *152*, 155–163. [[CrossRef](#)]
61. Li, S.; Xie, L.; He, M.; Hu, X.; Luo, G.; Chen, C.; Zhu, Z. Metal-Organic frameworks-derived bamboo-like CuO/In₂O₃ heterostructure for high-performance H₂S gas sensor with low operating temperature. *Sens. Actuators B Chem.* **2020**, *310*, 127828. [[CrossRef](#)]
62. Kumar, N.; Čapek, J.; Haviar, S. Nanostructured CuWO₄/WO₃- films prepared by reactive magnetron sputtering for hydrogen sensing. *Int. J. Hydrog. Energy* **2020**, *45*, 18066–18074. [[CrossRef](#)]
63. Peng, F.; Yu, W.; Lu, Y.; Sun, Y.; Fu, X.; Hao, J.M.; Chen, X.; Cong, R.; Dai, N. Enhancement of low-temperature gas-sensing performance using sub-stoichiometric WO_{3-x} Modified with CuO. *ACS Appl. Mater. Int.* **2020**, *12*, 41230–41238. [[CrossRef](#)]
64. Kim, J.-H.; Mirzaei, A.; Zheng, Y.; Lee, J.-H.; Kim, J.-Y.; Kim, H.W.; Kim, S.S. Enhancement of H₂S sensing performance of p-CuO nanofibers by loading p-reduced graphene oxide nanosheets. *Sens. Actuators B Chem.* **2019**, *281*, 453–461. [[CrossRef](#)]
65. Kim, Y.; Lee, S.; Song, J.G.; Ko, K.Y.; Woo, W.J.; Lee, S.W.; Park, M.; Lee, H.; Lee, Z.; Choi, H.; et al. 2D Transition metal dichalcogenide heterostructures for p-and n-type photovoltaic self-powered gas sensor. *Adv. Funct. Mater.* **2020**, *30*, 2003360. [[CrossRef](#)]
66. Luo, Y.; Zhang, D.; Fan, X. Hydrothermal Fabrication of Ag-Decorated MoSe₂/Reduced Graphene Oxide Ternary Hybrid for H₂S Gas Sensing. *IEEE Sens. J.* **2020**, *20*, 13262–13268. [[CrossRef](#)]
67. Shokri, A.; Salami, N. Gas sensor based on MoS₂ monolayer. *Sens. Actuators B Chem.* **2016**, *236*, 378–385. [[CrossRef](#)]
68. Zhang, D.; Wu, J.; Cao, Y. Ultrasensitive H₂S gas detection at room temperature based on copper oxide/molybdenum disulfide nanocomposite with synergistic effect. *Sens. Actuators B Chem.* **2019**, *287*, 346–355. [[CrossRef](#)]
69. Li, D.; Qin, L.; Zhao, P.; Zhang, Y.; Liu, D.; Liu, F.; Kang, B.; Wang, Y.; Song, H.; Zhang, T.; et al. Preparation and gas-sensing performances of ZnO/CuO rough nanotubular arrays for low-working temperature H₂S detection. *Sens. Actuators B Chem.* **2018**, *254*, 834–841. [[CrossRef](#)]
70. Yeh, B.-Y.; Jian, B.-S.; Wang, G.-J.; Tseng, W.J. CuO/V₂O₅ hybrid nanowires for highly sensitive and selective H₂S gas sensor. *RSC Adv.* **2017**, *7*, 49605–49612. [[CrossRef](#)]
71. Zhu, L.; Zeng, W. Physical, Room-temperature gas sensing of ZnO-based gas sensor: A review. *Sens. Actuators A Phys.* **2017**, *267*, 242–261. [[CrossRef](#)]
72. Zhang, J.; Liu, X.; Neri, G.; Pinna, N. Nanostructured Materials for Room-Temperature Gas Sensors. *Adv. Mater.* **2016**, *28*, 795–831. [[CrossRef](#)]
73. Majhi, S.M.; Mirzaei, A.; WooKimab, H.; Kim, S.S.; Kim, T.W. Recent advances in energy-saving chemiresistive gas sensors: A review. *Nano Energy* **2021**, *79*, 105369. [[CrossRef](#)] [[PubMed](#)]
74. Liu, X.-L.; Zhao, Y.; Wang, W.-J.; Ma, S.-X.; Ning, X.-J.; Zhao, L.; Zhuang, J. Photovoltaic Self-Powered Gas Sensing: A Review. *IEEE Sens. J.* **2020**, *21*, 5628–5644. [[CrossRef](#)]
75. Meng, G.; Zhuge, F.; Nagashima, K.; Nakao, A.; Kanai, M.; He, Y.; Boudot, M.; Takahashi, T.; Uchida, K.; Yanagida, T. Nanoscale Thermal Management of Single SnO₂ Nanowire: Pico-Joule Energy Consumed Molecule Sensor. *ACS Sens.* **2016**, *1*, 997–1002. [[CrossRef](#)]
76. Kim, J.-H.; Mirzaei, A.; Bang, J.H.; Kim, H.W.; Kim, S.S. Selective H₂S sensing without external heat by a synergy effect in self-heated CuO-functionalized SnO₂-ZnO core-shell nanowires. *Sens. Actuators B Chem.* **2019**, *300*, 126981. [[CrossRef](#)]
77. Kim, J.; Kim, W.; Yong, K. CuO/ZnO Heterostructured Nanorods: Photochemical Synthesis and the Mechanism of H₂S Gas Sensing. *J. Phys. Chem. C* **2012**, *116*, 15682–15691. [[CrossRef](#)]
78. Park, S.; Kim, S.; Kheel, H.; Hyun, S.K.; Jin, C.; Lee, C. Enhanced H₂S gas sensing performance of networked CuO-ZnO composite nanoparticle sensor. *Mater. Res. Bull.* **2016**, *82*, 130–135. [[CrossRef](#)]
79. Wang, T.-S.; Wang, Q.-S.; Zhu, C.-L.; Ouyang, Q.-Y.; Qi, L.-H.; Li, C.-Y.; Xiao, G.; Gao, P.; Chen, Y.-J. Synthesis and enhanced H₂S gas sensing properties of α-MoO₃/CuO p-n junction nanocomposite. *Sens. Actuators B Chem.* **2012**, *171–172*, 256–262. [[CrossRef](#)]
80. Arafat, M.M.; Dinan, B.; Akbar, S.A.; Haseeb, A.S.M.A. Gas Sensors Based on One Dimensional Nanostructured Metal-Oxides: A Review. *Sensors* **2012**, *12*, 7207–7258. [[CrossRef](#)]
81. Choi, K.J.; Jang, H.W. One-Dimensional Oxide Nanostructures as Gas-Sensing Materials: Review and Issues. *Sensors* **2010**, *10*, 4083–4099. [[CrossRef](#)]

82. Huang, J.; Wan, Q. Gas Sensors Based on Semiconducting Metal Oxide One-Dimensional Nanostructures. *Sensors* **2009**, *9*, 9903–9924. [[CrossRef](#)]
83. Li, T.; Zeng, W.; Wang, Z. Quasi-one-dimensional metal-oxide-based heterostructural gas-sensing materials: A review. *Sens. Actuators B Chem.* **2015**, *221*, 1570–1585. [[CrossRef](#)]
84. Hwang, I.-S.; Choi, J.-K.; Kim, S.-J.; Dong, K.-Y.; Kwon, J.-H.; Ju, B.-K.; Lee, J.-H. Enhanced H₂S sensing characteristics of SnO₂ nanowires functionalized with CuO. *Sens. Actuators B Chem.* **2009**, *142*, 105–110. [[CrossRef](#)]
85. Shao, F.; Hoffmann, M.W.G.; Prades, J.D.; Zamani, R.; Arbiol, J.; Morante, J.R.; Varechkina, E.; Rumyantseva, M.; Gaskov, A.; Giebelhaus, I.; et al. Heterostructured p-CuO (nanoparticle)/n-SnO₂ (nanowire) de-vices for selective H₂S detection. *Sens. Actuators B Chem.* **2013**, *181*, 130–135. [[CrossRef](#)]
86. Choi, K.-I.; Kim, H.-J.; Kang, Y.C.; Lee, J.-H. Ultrasensitive and ultrasensitive detection of H₂S in highly humid atmosphere using CuO-loaded SnO₂ hollow spheres for real-time diagnosis of halitosis. *Sens. Actuators B Chem.* **2014**, *194*, 371–376. [[CrossRef](#)]
87. Ramgir, N.S.; Goyal, C.; Sharma, P.; Goutam, U.; Bhattacharya, S.; Datta, N.; Kaur, M.; Debnath, A.; Aswal, D.; Gupta, S. Selective H₂S sensing characteristics of CuO modified WO₃ thin films. *Sens. Actuators B Chem.* **2013**, *188*, 525–532. [[CrossRef](#)]
88. Wang, X.; Li, S.; Xie, L.; Li, X.; Lin, D.; Zhu, Z. Low-temperature and highly sensitivity H₂S gas sensor based on ZnO/CuO composite derived from bimetal metal-organic frameworks. *Ceram. Int.* **2020**, *46*, 15858–15866. [[CrossRef](#)]
89. Sui, L.; Yu, T.; Zhao, D.; Cheng, X.; Zhang, X.; Wang, P.; Xu, Y.; Gao, S.; Zhao, H.; Gao, Y.; et al. In situ deposited hierarchical CuO/NiO nanowall arrays film sensor with enhanced gas sensing performance to H₂S. *J. Hazard. Mater.* **2020**, *385*, 121570. [[CrossRef](#)]
90. Fan, C.; Sun, F.; Wang, X.; Majidi, M.; Huang, Z.; Kumar, P.; Liu, B. Enhanced H₂S gas sensing properties by the optimization of p-CuO/n-ZnO composite nanofibers. *J. Mater. Sci.* **2020**, *55*, 7702–7714. [[CrossRef](#)]
91. Zhao, Y.; Zhang, J.; Wang, Y.; Chen, Z. A Highly Sensitive and Room Temperature CNTs/SnO₂/CuO Sensor for H₂S Gas Sensing Applications. *Nanoscale Res. Lett.* **2020**, *15*, 1–8. [[CrossRef](#)]